Auton Robot (2014) 36:181–198
DOI 10.1007/s10514-013-9345-0

Scan matching SLAM in underwater environments

Angelos Mallios · Pere Ridao · David Ribas · Emili Hernández

Received: 28 February 2012 / Accepted: 5 June 2013 / Published online: 25 June 2013

Abstract This paper proposes a pose-based algorithm to solve the full simultaneous localization and mapping problem for autonomous underwater vehicle (AUV) navigating in unknown and possibly unstructured environments. The proposed method first estimates the local path traveled by the robot while forming the acoustic image (scan) with range data coming from a mono-beam rotating sonar head, providing position estimates for correcting the distortions that the vehicle motion produces in the scans. Then, consecutive scans are cross-registered under a probabilistic scan matching technique for estimating the displacements of the vehicle including the uncertainty of the scan matching result. Finally, an augmented state extended Kalman filter estimates and keeps the registered scans poses. No prior structural information or initial pose are considered. The viability of the proposed approach has been tested reconstructing the trajectory of a guided AUV operating along a 600 m path within a marina environment.

Electronic supplementary material The online version of this article (doi:10.1007/s10514-013-9345-0) contains supplementary material, which is available to authorized users.

A. Mallios (✉) · P. Ridao · D. Ribas
Department of Computer Engineering, Universitat de Girona, Campus de Montilivi, Edifici P4, 17003 Girona, Spain
e-mail: amallios@eia.udg.edu

P. Ridao
e-mail: pere@eia.udg.edu

D. Ribas
e-mail: dribas@eia.udg.edu

E. Hernández
Autonomous Systems Laboratory, ICT Centre, CSIRO, 1 Technology Court, Pullenvale 4069, QLD, Australia
e-mail: Emili.Hernandez@csiro.au

Keywords Simultaneous localization and mapping · Underwater robotics · Autonomous underwater vehicle · Scan matching · Pose estimation · Sonar imaging

1 Introduction

In spite of recent advances in autonomous underwater vehicles (AUVs) navigation techniques, robustly solving their localization in unstructured and unconstrained areas is still a challenging problem. Compared to towed systems or remotely operated vehicles (ROVs), AUVs are very stable and efficient platforms in many cases. Combined with precise navigation, large area surveys with desirable coverage can be achieved and high resolution and accurate data product can be delivered. However, as for every platform, the order of the final product accuracy is highly correlated with the platform's navigation estimation. In contrast to surface vehicles that have direct access to global positioning system (GPS), navigation of underwater vehicles is very challenging. Due to the fundamental properties of the water column, high frequency signals (such those from GPS) do not penetrate below the surface (Barclay 2003) and AUVs do not have direct access to them while underwater. To achieve the best possible navigation accuracy, a common technique is to deploy a set of acoustic transponders in the area of interest, and through triangulation, the vehicle's pose can be estimated with centimeter accuracy. The disadvantage of such a technique is that the deployment, calibration, recovery of the transponders and the relatively small area of coverage consumes costly ship time and complicates the operations (Kinsey et al. 2006; Stutters et al. 2008).

In the last 20 years of research, a number of studies in mobile robotics have developed techniques to address the autonomous localization problem with very promising

results. In particular, simultaneous localization and mapping (SLAM) techniques have been broadly and successfully applied to indoor and outdoor environments. A number of algorithms exist that propose to solve the SLAM problem, with notable achievements mostly in land mobile robotics (Bailey and Durrant-Whyte 2006; Lu et al. 2009). Comparatively, there has been little work done in the field of underwater SLAM mostly due to the complexity of the environment and the difficulty in conducting field experiments.

This paper is a contribution in that area, proposing a pose-based algorithm to solve the full SLAM problem of an AUV navigating in an unknown and possibly unstructured environment. The technique incorporates two extended Kalman filter (EKF) running in parallel. The first estimates the dead reckoning displacements of the vehicle estimated from a Doppler velocity log (DVL) and an attitude and heading reference system (AHRS). The second is an augmented state EKF (ASEKF) which is updated from probabilistic scan matching with range and bearing measurements gathered from a mechanically scanned imaging sonar (MSIS).

The proposed method has been tested with a real world dataset in a structured environment. The dataset is an experimental survey in an abandoned marina where the AUV operates along a 600 m path with access to a differential global positioning system (DGPS) for ground truth and has been previously used by the authors in the works of Ribas et al. (2008) and Hernandez et al. (2009). The main and important difference from the first former work is that now we do not seek to extract features from the environment to estimate the relative vehicle position but we apply scan matching between scan points. Although the results presented here are very similar, the main contribution of the new technique is that it has the potential to be applied in an unstructured environment. The second former work also uses scan matching but not in a SLAM framework. By incorporating scan matching into the SLAM framework, the results show substantial improvements in trajectory correction and map reconstruction.

The rest of this paper is organized as follows: In the next section we review related work in the underwater domain. Section 3 describes an algorithm for dealing with the distortion in the acoustic images caused by the vehicle's motion. Section 4 details the probabilistic scan matching algorithm that we apply, followed by its uncertainty estimation in Sect. 5. Both are essential parts of the proposed SLAM algorithm which is described in Sect. 6. Section 7 reports the experimental setup and results, and in Sect. 8 we discuss the results and the directions for future work. Finally, we conclude in Sect. 9.

2 Related field work

The environment plays a significant role in the performance of a robotic system. In contrast to the mobile robotics that in most cases have the advantage of long range visibility and high frequency communications, including GPS signals, the perception of underwater vehicles (without any external infrastructure) is limited to vision and sonar sensors.

Vision sensors are a common choice among many researchers for a variety of reasons: They are relatively inexpensive, can provide large amounts of high resolution information with high refresh rate, and well-known techniques from decades of research on computer vision can be applied. The last years have witnessed successful real-world implementations (to mention just few: Eustice et al. 2005; Ferrer et al. 2007; Singh et al. 2007; Johnson-Roberson et al. 2010). Generally speaking, in underwater visual SLAM a number of overlapping pictures of the sea floor are grabbed and features are identified. From the displacement of features in the images, the movement of the AUV can be estimated and at the same time, the registered images are combined producing a photo-mosaic of the traveled area (Garcia et al. 2006; Mahon et al. 2008; Pizarro et al. 2010; Elibol et al. 2010). A number of oceanographic applications share the requirement for high resolution imaging of sites extending over hundreds of meters. These include fisheries habitats (Reynolds et al. 2001), coral reefs (Singh et al. 2004), hydrothermal vent sites (German et al. 2004), cold seep sites (Hill et al. 2004) and shipwrecks or archaeological significance sites (Eustice et al. 2005; Foley et al. 2009; Mahon et al. 2011). On the other hand, underwater vision is limited to a few meters ($<$10 m) and can be easily disturbed by turbulence, floating sediment or lighting conditions.

It is very common to use low frequency sonar sensors for long range sensing rather than ultra high resolution devices (like vision or laser scanners) which suffer due to the rapid attenuation of high frequencies in the water. In comparison with vision, sonar sensors are generally more expensive, offer limited information and medium to low resolution and refresh rate. However, acoustic sonar frequencies can penetrate further in the water column and are not prone to turbidity, thus sonar sensors can provide information even in bad visibility conditions (e.g. $>$150 m for a forward looking sonar). The driving force for research with sonar sensors is straightforward; sonar sensors provide long range perception underwater that is needed for obstacle avoidance, path planning, navigation and mapping, which are very important modules for real autonomous robots.

Although there are still few works in underwater sonar-based SLAM, they are promising. Several feature based methods have been reported using point features extracted from different types of imaging sonars (Carpenter 1998; Leonard et al. 2001; Leonard and Feder 2001; Williams et al. 2001; Newman et al. 2003; Tena et al. 2004; Walter et al. 2008) and line features extracted from a mechanically scanned imaging sonar probabilistic iterative correspondence (MSISpIC) in the structured environment of a marina

(Ribas et al. 2008). Nevertheless, in a natural underwater environment it may be difficult to recognize features via sonar. Often their appearance changes dramatically depending on the point of view, making it extremely difficult to extract robust features. For this reason, some researchers have focused their efforts on using featureless methods like occupancy grids and scan matching.

In order to construct a 3D map of a sinkhole, Fairfield et al. (2007) proposed a Rao-Blackwellized particle filter (PF) based SLAM algorithm that builds an occupancy grid using range measurements from multiple pencil beam sonars. In Barkby et al. (2009), the authors worked with a multibeam sonar profiler producing 2.5D bathymetric maps and also used PF-based SLAM, but representing the environment, as an elevation map distributed across the ancestry of a given particle. In White et al. (2010), FastSLAM and occupancy grid map were used in order to map flooded ancient cisterns, using a small ROV equipped with a MSIS.

Another featureless technique that has attracted attention in recent years is sonar registration, also known as scan matching. Although a large literature exists reporting successful applications of scan matching and SLAM to mobile robots, very few attempts have been made to use sonar scan matching in underwater applications and even fewer use them in a SLAM framework.

In underwater scan matching algorithms the work from Castellani et al. (2004) proposed a non-probabilistic variation of iterative closest point (ICP), to achieve on-line performance for registering multiple views captured with a 3D acoustic camera. Also, Hernandez et al. (2009) proposed the MSISpIC that deals with data gathered by an AUV utilizing MSIS. Their work is based on the probabilistic iterative correspondence (pIC) algorithm (Montesano et al. 2005) but takes into account the distortions in the acoustic image due to vehicle motion. In Bülow et al. (2010) a 2D scan matching method is presented that is based on spectral registration of rendered scan data, which the authors recently extended to 3D sonar images (Bülow and Birk 2011).

Scan matching can delay the drift that occurs from the dead reckoning estimation, but is unable to bound it over time. For this reason, recent studies have been developed that combine SLAM and sonar scan matching underwater with notable results. In Roman and Singh (2005), an ICP variant is used for registering bathymetric sub-maps gathered with a multibeam sonar profiler. With a MSIS as the main sonar sensor, Mallios et al. (2010) incorporated point-to-point scan matching in an ASEKF that bounds the drift, and tested in the structured underwater environment of a marina. With the same dataset, Burguera et al. (2010) used an iterated EKF to estimate the trajectory of the AUV.

In this paper we focus on a SLAM algorithm incorporating scan matching techniques aided from a MSIS. Each new pose of a scan is maintained in an ASEKF and is compared with previous scans that are in the nearby area. If there is enough data overlapping, a new scan match will put a constraint between the poses updating the ASEKF. These constraints help to identify and close the loops which correct the entire trajectory, thus bounding the drift.

3 Working with acoustic images from a MSIS

Most mobile robots utilize laser technology sensors, which beside their high accuracy range, have two major advantages: they gather each scan almost instantaneously and the beams angles can be considered almost perfect. However, when using acoustic or ultrasonic range finders these advantages are no longer valid because of their lower angular resolution and the sparsity of the readings.

Underwater vehicles utilize acoustic sonar instead of laser sensors since light propagation in water is very poor. Commercially available underwater sonar sensors cover a scan sector by emitting acoustic beams either with a mechanical head that rotates at fixed angular steps or simultaneously by a multibeam sonar head. The new multibeam forward looking sonar sensors that have been introduced in the market, have improved resolution and refresh rates. However, still relatively few of them are deployed in the field and their scan sectors are limited to 120 deg. On the other hand, MSIS have been a very popular choice for many years now, offering full 360 deg scan sectors. Their main drawbacks, which we will address in this section, comes from the fact that they give noisy measurements and use relatively slow rotated mechanical heads. At each step, a beam is emitted and received, measuring the intensities of the acoustic reflections from the obstacles found across its path. Acquiring a scan of a complete sector takes several seconds, in which time the motion of the vehicle causes distortions in the final acoustic image. For this reason, it is necessary to take into account the robot pose when the beam was grabbed (Fig. 1).

To address these problems, we introduce the *ScanGrabbing* algorithm whose role is to collect all the beams that form a full 360 deg sonar scan sector (referred as a *scan* from now on), filter them to remove noise, and remove the distortion in the final scan due to the vehicle motion. Next, we will present the three major parts that ScanGrabbing algorithm consisting of: (1) Beam segmentation, (2) relative vehicle localization, and (3) scan forming.

3.1 Beam segmentation and range detection

We can represent a full scan as a polar acoustic image composed of beams (Fig. 2a). Each beam has a particular bearing angle value with respect to the MSIS sensor and a set of intensity measurements acquired at known intervals along the beam path. The angle corresponds to the orientation of

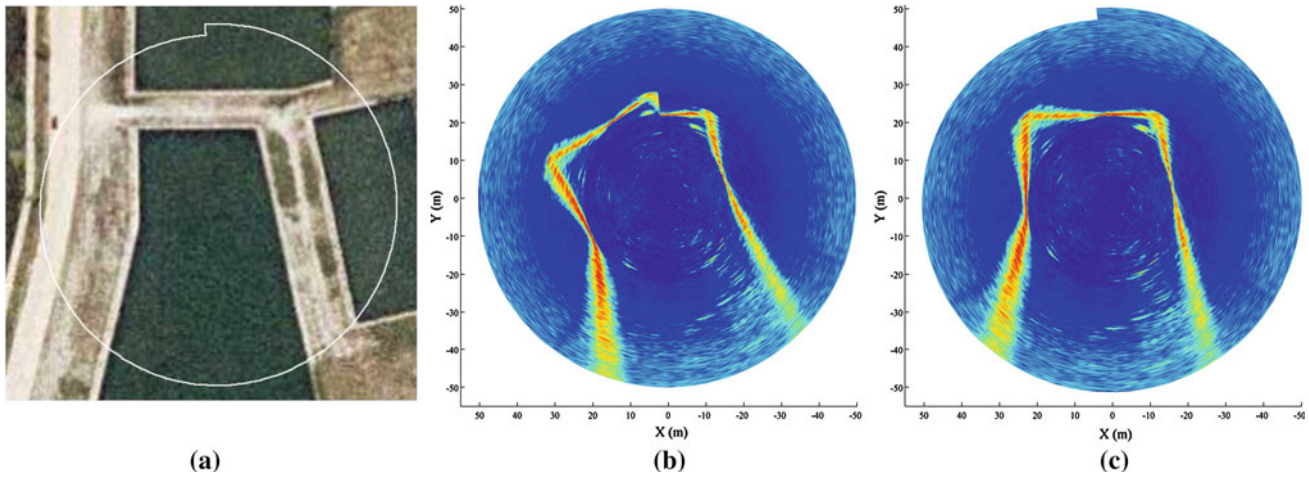

Fig. 1 Effect of motion induced-distortion on acoustic images: **a** orthophoto map of the real environment where sonar data was gathered. **b** The sonar data represented in Cartesian coordinates. **c** Undistorted image obtained after taking into account the vehicle motion

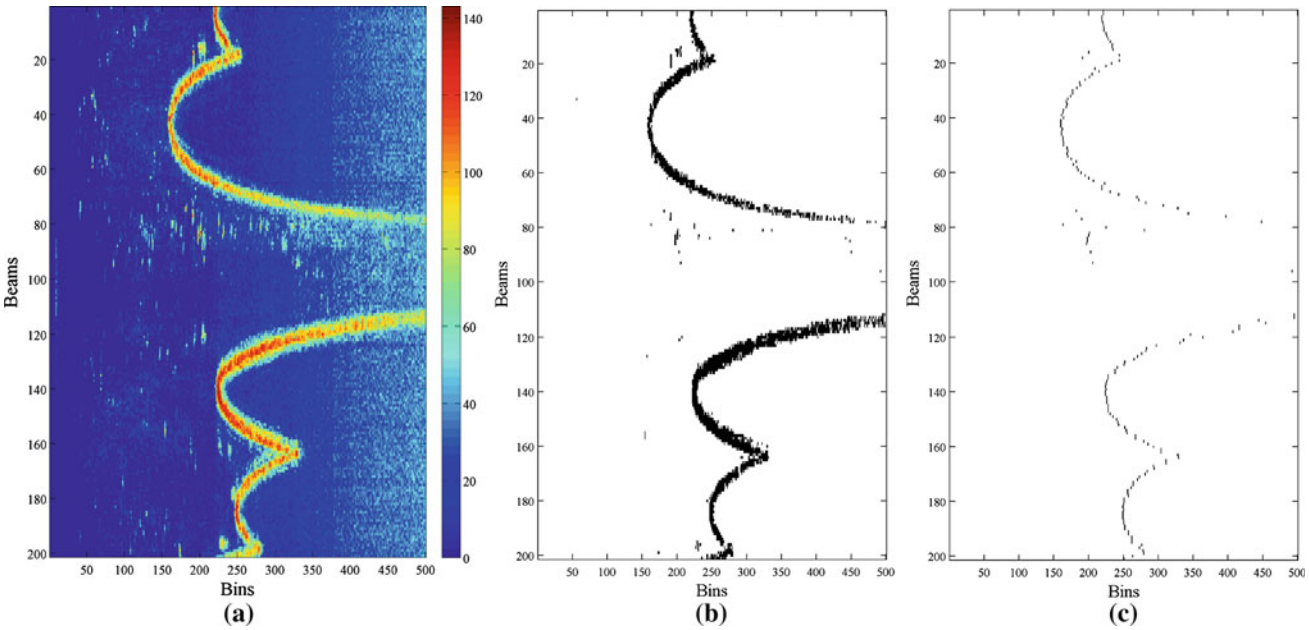

Fig. 2 MSIS beam segmentation: **a** raw data represented in polar coordinates. **b** Data after applying a threshold. **c** Selection of the local maxima bins of each beam

the sensor head when the beam was emitted. The acoustic linear image corresponding to one beam is returned as an array of acoustic intensities detected at a certain distance. Due to the noisy nature of the acoustic data, to obtain a range measurement the beam is segmented in two steps. First, only those bins with an intensity value over a threshold are selected and stored. This procedure separates the acoustic imprint left by an object in the image from the noisy background data (Fig. 2b). The second step is to select among the beam's thresholded data those bins that are local maxima and satisfy a "minimum distance between them" criterion. This means that if two or more of these bins are too close within the beam, they should correspond to the detection of the same object and hence are redundant. Then, the ones with the lowest intensity value are discarded (see the result in Fig. 2c). The selected local high-intensity bins are the ones that most likely correspond to objects present in the scene.

3.2 Relative vehicle localization

Since MSIS needs a considerable period of time to obtain a complete scan (∼14 s), motion induces a distortion in the acoustic image when the vehicle does not remain static, which is very common in water (Fig. 1). To deal with this problem, it is necessary to know the vehicle's pose at the beam transmission and reception time. As most of the AUVs

are moving with relatively low speeds, the time difference between beam transmission and reception can be neglected and only the reception pose is considered. Therefore, we define an initial coordinate system I_c to reference all the range measurements belonging to the same scan. In order to reduce the influence of the motion uncertainties to the scan, as Burguera et al. (2008) suggested, we set this reference frame at the robot pose where the center beam of the current scan was read.

The localization system used in this work to estimate the vehicle motion, follows the navigation system described in Ribas et al. (2008). In this system, an AHRS provides attitude measurements and a DVL unit including a pressure sensor are used to estimate the robot's velocity and depth during the scan. All measurements happen asynchronously with the MSIS beams arriving at 30 Hz rate while DVL and AHRS readings arrive with frequency of 1.5 and 10 Hz respectively. The AUV used in this work is very stable in roll and pitch and during the experiments it performed survey patterns at constant speed. Therefore, a simple four degrees of freedom (DOF) constant velocity kinematics model is used to predict vehicle motion. An EKF is used to estimate the robot's pose whenever a sonar beam is received and to update the model prediction each time a new DVL or AHRS measurement arrives. An analytical description of the system model is presented next.

The information of the system at step k is stored in the state vector $\mathbf{x}_k$ with estimated mean $\hat{\mathbf{x}}_k$ and covariance $\mathbf{P}_k$:

$$\hat{\mathbf{x}}_k = \begin{bmatrix} \eta^B \\ \nu^R \end{bmatrix}, \quad \mathbf{P}_k = E\left[\left(\mathbf{x}_k - \hat{\mathbf{x}}_k\right)\left(\mathbf{x}_k - \hat{\mathbf{x}}_k\right)^T\right] \tag{1}$$

with:

$$\eta^B = [x, y, z, \psi]^T, \quad \nu^R = [u, v, w, r]^T \tag{2}$$

where, as defined in Fossen (1994), η^B is the position (x, y, z) and attitude (ψ) vector referenced to a base frame B and ν^R is the linear (u, v, w) and angular (r) velocity vector referenced to the robot's coordinate frame R. The coordinate frame B is chosen coincident with I but aligned with the North, hence it is straightforward the integration of the compass measurements. Finally, the model prediction and update is carried out as detailed below.

3.2.1 Prediction

The vehicle's movement prediction at step k with a time step Δt is performed using the following 4-DOF constant velocity kinematic model:

$$\mathbf{x}_k = f(\mathbf{x}_{k-1}, n_k) \longrightarrow \begin{bmatrix} \eta_k^B \\ \nu_k^R \end{bmatrix} = \begin{bmatrix} \eta_{k-1}^B + R\left(\eta_{k-1}^B\right)\left(\nu_{k-1}^R \Delta t + n_k \frac{\Delta t^2}{2}\right) \\ \nu_{k-1}^R + n_k \Delta t \end{bmatrix} \tag{3}$$

with:

$$R(\eta) = \begin{bmatrix} cos(\psi) & -sin(\psi) & 0 & 0 \\ sin(\psi) & cos(\psi) & 0 & 0 \\ 0 & 0 & 1 & 0 \\ 0 & 0 & 0 & 1 \end{bmatrix} \tag{4}$$

In this model the velocity is considered to be constant with a velocity perturbation that is modeled as the integral of a zero-mean white Gaussian noise n_k. The covariance matrix $\mathbf{Q}_k$ of this acceleration noise is assumed diagonal and in the same order of magnitude of the maximum acceleration increment that the robot may experience over a sample period. The estimate of the state is obtained with the standard EKF prediction equations.

3.2.2 Update using DVL or AHRS measurements

Whenever new velocities or heading measurements are available from the DVL or AHRS sensor, the model prediction is updated using the standard Kalman filter equations:

$$\mathbf{z}_{DVL,k} = [u_{b,w}, v_{b,w}, w_{b,w}, z_{depth}]^T, \quad \mathbf{z}_{AHRS,k} = [\psi] \tag{5}$$

where subindex b or w stands for bottom tracking velocity or water layer tracking velocity. The measurement model becomes:

$$\mathbf{z}_{DVL,k} = \mathbf{H}_{DVL}\mathbf{x}_k + w_k, \quad \mathbf{z}_{AHRS,k} = \mathbf{H}_{AHRS}\mathbf{x}_k + w_k \tag{6}$$

$$\mathbf{H}_{DVL} = \begin{bmatrix} 0 & 0 & 0 & 0 & 1 & 0 & 0 & 0 \\ 0 & 0 & 0 & 0 & 0 & 1 & 0 & 0 \\ 0 & 0 & 0 & 0 & 0 & 0 & 1 & 0 \\ 0 & 0 & 1 & 0 & 0 & 0 & 0 & 0 \end{bmatrix},$$

$$\mathbf{H}_{AHRS} = \begin{bmatrix} 0 & 0 & 0 & 1 & 0 & 0 & 0 & 0 \end{bmatrix} \tag{7}$$

where w_k (measurement noise) is a zero-mean white Gaussian noise.

3.3 Scan forming

The navigation system presented above is able to estimate the robot's pose, but the uncertainty will grow without limit due to its dead-reckoning nature. However, we are only interested in the robot's relative position and uncertainty within a scan with respect to the center of that scan (I_c frame, Fig. 3). For this reason the filter is starting with the position and its uncertainty to zero whenever a new beam is emitted, which keeps the consecutive beams measurements statistically independent and uncorrelated.

The filter is initialized with the yaw (ψ) value from the attitude sensor because it represents an absolute angle with respect to the magnetic North. In this way, the modified filter

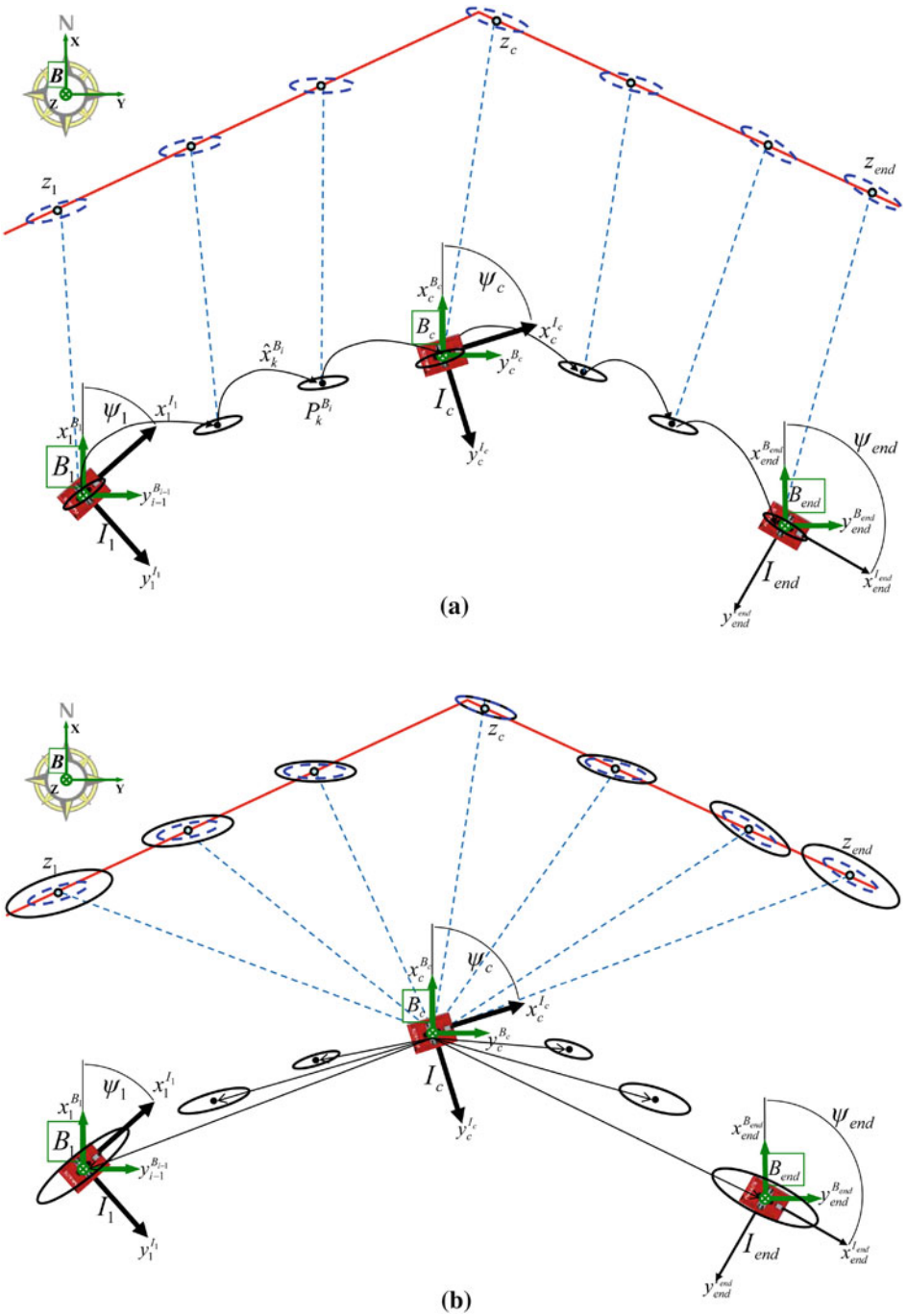

Fig. 3 The scan forming process, simplified for clarity. **a** Each vehicle pose corresponds with the acquisition of a beam and is represented with respect to a new North-aligned reference frame. The arcs between poses represent the relative displacements. **b** The beams in a full scan are then referenced to the I_c frame, which corresponds with the position at the center of the trajectory. The uncertainty of the dead-reckoning process is distributed accordingly and propagated to the scan points

provides the robot's relative displacements (and their uncertainties) between consecutive beam acquisitions. With these available, it is possible to compose the measurements with the vehicle motion to diminish the effect of distortions, while referencing them to the new frame I_c to produce a better uncertainty distribution (see Burguera et al. 2008).

It is very common in robotics that a dead reckoning system provides the relative angle and displacement between consecutive poses together with their uncertainties. Then, it is straightforward to form a trajectory from several consecutive translations and to reference them to any desired frame by means of compounding or inverse transformations, as described in Smith et al. (1990) and applied in Burguera et al. (2008).

However, absolute compass readings are not in the same reference frame as the corresponding relative displacements, hence we propose bellow a different approach to form a scan with respect to a common coordinate frame I.

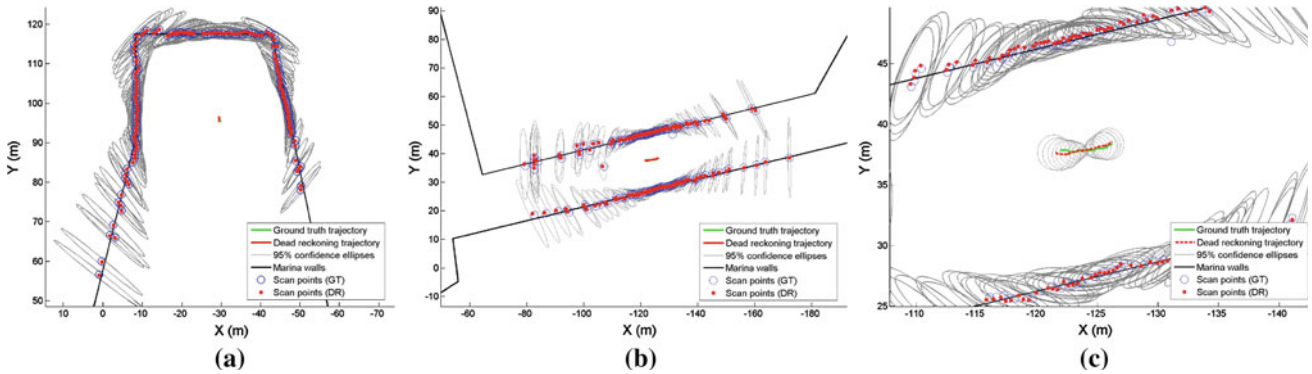

Fig. 4 Scan forming examples over their corresponding ground truth reference positions: **a** the scan from Fig. 1. **b** Scan from a corridor of the same environment. **c** Magnification showing the trajectory of the dead reckoning and the ground truth

Let,

- $\mathbf{z}_i^{I_i} \equiv N(\hat{\mathbf{z}}_i^{I_i}, \mathbf{P}_{z_i})$ be the measurement points modeled as Gaussian random variables (GRVs), of the scan to be formed in the I_i frame corresponding to the related robot pose at step i,
- B_i be the North-aligned frame sharing the same origin as I_i,
- $\mathbf{x}_i^{B_i} \equiv N(\hat{\mathbf{x}}_i^{B_i}, \mathbf{P}_{x_i})$ be the robot state and uncertainty from the dead reckoning EKF, with $\hat{\mathbf{x}}_i^{B_i} = [x_i, y_i, \psi_i]^T$,
- $\mathbf{d}_i^{B_i} \equiv N(\hat{\mathbf{d}}_i^{B_i}, \mathbf{P}_{d_i})$ be the robot displacement between time step $i-1$ and i, where $\hat{\mathbf{d}}_i^{B_i} = [x_i, y_i, 0]^T$ are elements from the robot state $\hat{\mathbf{x}}_i^{B_i}$ and $\mathbf{P}_{d_i}$ the corresponding submatrix from its covariance matrix, and
- $\mathbf{r}_i^{B_i} \equiv N(\hat{\mathbf{r}}_i^{B_i}, \mathbf{P}_{r_i})$ be the rotation transformation between the robot coordinate frame I_i with the corresponding North-aligned frame B_i, where $\hat{\mathbf{r}}_{I_i}^{B_i} = [0, 0, \psi_i]^T$ are elements from the robot state $\hat{\mathbf{x}}_i^{B_i}$ and $\mathbf{P}_{r_i}$ the corresponding submatrix from its covariance matrix,

then, we can form the scan with respect to the center frame I_c (Fig. 3), as follows:

$$\mathbf{z}_i = \begin{cases} \mathbf{z}_i & i = c \\ \ominus \mathbf{r}_{I_c}^{B_c} \oplus \mathbf{D}_{I_c}^{B_c} \oplus \mathbf{r}_{I_i}^{B_i} \oplus \mathbf{z}_i^{I_i} & i \neq c \end{cases} \tag{8}$$

where

$$\mathbf{D}_{I_c}^{B_c} = \sum_{j=c}^{i-1} sign\,(i-c)\,\mathbf{d}_j^{B_j} \tag{9}$$

is the relative robot pose referenced to B_c where point $\mathbf{z}_i$ was observed. Because all the consecutive robot displacements $\mathbf{d}_j^{B_j}$ are represented in a North-aligned frame $\left(B_j\right)$, a simple linear vector addition operation is enough to compute $\mathbf{D}_{I_c}^{B_c}$.

Figure 4a, b illustrate the results of the scan-forming algorithm by showing as an example, two scans from a real environment. The readings shown correspond to the acoustic images in Fig. 1 and to the corridor part (see Sect. 7). The reference point of each scan has been placed at the corresponding ground truth position in order to highlight the coherence of the scans compared with the ground truth trajectory. The scan trajectory of Fig. 4b is shown in more detail in Fig. 4c with the 95 % confidence ellipses. It can be easily seen that the proposed scan forming algorithm builds the scan in agreement with the ground truth and that the absolute drift of the dead reckoning system of the vehicle during the scan is small due to the short time required for a complete scan. The histogram of the absolute error of all the scans is shown in the results section (Fig. 8) and is comparable to the DGPS error that we use as a ground truth. For this reason, can be assumed that the deformations still remaining after the composition of the measurements with the dead-reckoning trajectory are negligible. Therefore, after the creation of a scan, it is considered to be rigid and it is not modified during the SLAM process.

4 Probabilistic scan matching

Scan matching is a technique that estimates the robot's relative displacement between two poses by maximizing the overlap between range scans normally gathered with a laser or sonar sensor.

In general, a number of beams are emitted from a sensor to cover a certain sector of an area (scan) either simultaneously or sequentially from a rotating transducer head. Given a reference scan S_{ref}, a new scan S_{new} and the vehicle's initial displacement estimation $\mathbf{q}_0$ between them, the objective of scan matching methods is to obtain a better estimate of the real displacement $\mathbf{q} = (x, y, \theta)$ (Fig. 5).

Several scan matching algorithms exist with most of them being variations of the ICP algorithm. The geometric representation of a scan in the conventional ICP algorithm does not model the uncertainty of the sensor measurements.

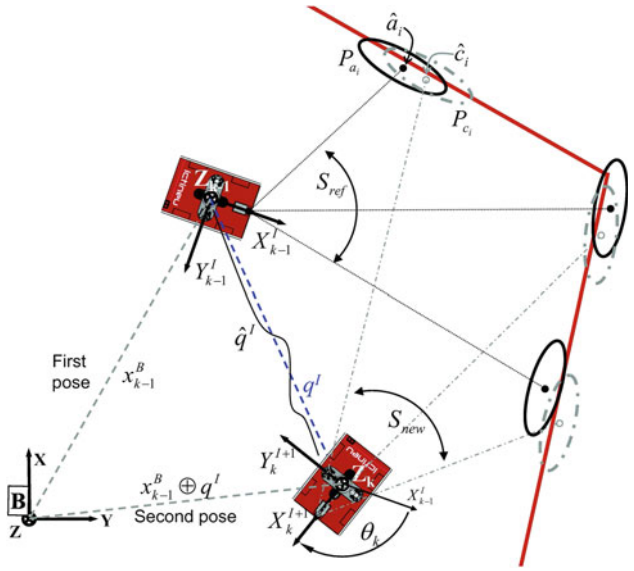

Fig. 5 Scan matching problem description

Algorithm 1 The modified pIC algorithm

1: $\hat{\mathbf{q}}_{pIC} = pIC(S_{ref}, S_{new}, \hat{\mathbf{q}}, \mathbf{P}_q)$ {
2: $k = 0$
3: $m = size(S_{new})$
4: $\hat{\mathbf{q}}_k = \hat{\mathbf{q}}$
5: **do** {
6: **for**$(i = 0; m; i++)$ {
7: $\hat{\mathbf{n}}_i = \hat{\mathbf{q}}_k \oplus \hat{\mathbf{c}}_i$
8: $A = \{\mathbf{r}_i \in S_{ref} / D_M^2(\mathbf{r}_i, \mathbf{n}_i) \leq \chi^2_{2,\alpha}\}$
9: $\hat{\mathbf{a}}_i = arg\ min_{\mathbf{r}_i \in A}\{D_M^2(\mathbf{r}_i, \mathbf{n}_i)\}$
10: $\hat{\mathbf{e}}_i = \hat{\mathbf{a}}_i - \hat{\mathbf{q}}_k \oplus \hat{\mathbf{c}}_i$
11: $\mathbf{P}_{e_i} = \mathbf{P}_{a_i} + \mathbf{J}_q \mathbf{P}_q \mathbf{J}_q^T + \mathbf{J}_c \mathbf{P}_{c_i} \mathbf{J}_c^T$
12: }
13: $\hat{\mathbf{q}}_{min} = arg\ min_{\mathbf{q}} \left\{ \frac{1}{2} \sum_{i=1}^{m} \left(\hat{\mathbf{e}}_i^T \mathbf{P}_{e_i}^{-1} \hat{\mathbf{e}}_i \right) \right\}$
14: **if**$(Convergence())$
15: $\hat{\mathbf{q}}_{pIC} = \hat{\mathbf{q}}_{min}$
16: **else** {
17: $\hat{\mathbf{q}}_{k+1} = \hat{\mathbf{q}}_{min}$
18: $k++$
19: }
20: }
21: **while**$(!Convergence()$ **and** $k < maxIterations)$
22: }

Correspondences between two scans are chosen based on the closest-point rule normally using the Euclidean distance. As pointed out in Montesano et al. (2005), this distance does not take into account that the points in the new scan which are far from the sensor, could be far from their corresponding point in the previous scan due to the sensor uncertainty. In other words, if the scan data is very noisy, two statistically compatible points could appear far enough, in terms of the Euclidean distance. This situation might prevent a possible association or even generate a wrong one, so Montesano et al. (2005) proposed the pIC algorithm which is a statistical extension of the ICP algorithm where the relative displacement as well as the observed points in both scans are modeled as GRVs. Because of the strong noise that characterize underwater sonar data, we choose to adapt pIC for the scan matching part of our algorithm. For a better understanding, the modified pIC is reproduced in Algorithm 1 and explained below in detail.

The inputs of the algorithm are the reference scan S_{ref} with points $\mathbf{r}_i$ $(i = 1 \ldots n)$, the new scan S_{new} with points $\mathbf{c}_i$ $(i = 1 \ldots m)$ and the initial relative displacement estimation $\hat{\mathbf{q}}_0$ with its covariance $\mathbf{P}_q$ (line 1). The following procedure is iteratively executed until convergence. First, the points of the new scan $(\mathbf{c}_i)$ are compounded with the robot displacement $(\mathbf{q}_k)$ (line 7). The result $(\mathbf{n}_i)$, is the set of points of the new scan projected to the same reference frame as the S_{ref}. Then, for each point $\mathbf{n}_i$, the set of statistically compatible points (A) is computed using the *Mahalanobis* distance and a certain confidence level α (line 8). From that, at line 9, the association point $\mathbf{a}_i$ is selected using the individual compatibility nearest neighbor (ICNN) criterion (Bar-Shalom, Y. and Fortmann T. E. 1988).

Given $\mathbf{q}_k \equiv N(\hat{\mathbf{q}}_k, \mathbf{P}_q)$, $\mathbf{c}_i \equiv N(\hat{\mathbf{c}}_i, \mathbf{P}_{c_i})$ and $\mathbf{r}_i \equiv N(\hat{\mathbf{r}}_i, \mathbf{P}_{r_i})$ are GRVs, the matching error $\mathbf{e}_i \equiv N(\hat{\mathbf{e}}_i, \mathbf{P}_{e_i})$ of the $\{\mathbf{a}_i, \mathbf{n}_i\}$ pairing can be computed as (lines 10-11):

$$\mathbf{e}_i = \mathbf{a}_i - \mathbf{n}_i = \mathbf{a}_i - \mathbf{q}_k \oplus \mathbf{c}_i \tag{10}$$

$$\hat{\mathbf{e}}_i \equiv \hat{\mathbf{a}}_i - \hat{\mathbf{q}}_k \oplus \hat{\mathbf{c}}_i \tag{11}$$

$$\mathbf{P}_{e_i} = \mathbf{P}_{a_i} + \mathbf{J}_q \mathbf{P}_q \mathbf{J}_q^T + \mathbf{J}_c \mathbf{P}_{c_i} \mathbf{J}_c^T \tag{12}$$

where

$$\mathbf{J}_q = \left. \frac{\partial\, \mathbf{a}_i - \mathbf{q}_k \oplus \mathbf{c}_i}{\partial\, \mathbf{q}_k} \right|_{\hat{\mathbf{q}}_k}, \quad \mathbf{J}_c = \left. \frac{\partial\, \mathbf{a}_i - \mathbf{q}_k \oplus \mathbf{c}_i}{\partial\, \mathbf{c}_i} \right|_{\hat{\mathbf{c}}_i} \tag{13}$$

$\mathbf{P}_{e_i}$ is the uncertainty of the matching error $(\mathbf{a}_i - \mathbf{n}_i)$ which is used to estimate the displacement $\hat{\mathbf{q}}_{min}$ through the minimization of the squared *Mahalanobis* distance of the matching error (line 13). This is done using non-linear least squares minimization method, iterating until convergence is achieved (lines 14–21).

5 Scan matching covariance estimation

Calculating the covariance of a measurement is essential when it has to be fused with other measurements in a stochastic framework like SLAM. Although ICP-style algorithms lead to very good estimations of the relative displacements and have been improved over the last decade, to the authors best knowledge, very few works exist which try to address the uncertainty of the estimation. Covariance estimation based on the environment and the uncertainties of the sensor model has been introduced in Lu (1995) and Pfister et al. (2002) but

as has been shown in Bengtsson and Baerveldt (2003), this estimation can be very optimistic in a number of cases. To overcome this problem they suggest two different methods, the *Hessian* and the *sampling* method. As was shown in the previous section, part of the scan matching algorithm is to define the error function (10) which is minimized by least-squares. Through the linearization of the error function, its Hessian matrix can be calculated and the covariance can be estimated by linear regression theory. The sampling method estimates the covariance matrix of a scan from a specific position by simulating and matching scans around the position. The authors conclude that the Hessian method is suitable for online estimation, being able to capture the shape but not the size of the covariance matrix. On the other hand, while the second method captures the correct size and shape of the covariance matrix, it can only be applied offline due to the computational cost.

In a SLAM framework, an approach similar to the offline method is used in Nieto et al. (2007) although in this case, only the initial guess of the displacement is sampled. An interesting approach for the uncertainty analysis, but for a 6-DOF spectral registration method, was introduced recently in Pfingsthorn et al. (2012). In Balsamo et al. (2006), the authors suggested that the method for estimating the covariance should be independent from the algorithm used for the minimization. They observed the paradox that different optimization methods may converge to the same minima, but led to seemingly different uncertainties without indicating which one is to be adopted. Based on the same observation, the uncertainty propagation independent from the minimization algorithm for the computer vision domain is shown in Haralick (1998). The method is based on the Hessian of the cost function with respect to the estimated displacement and the derivative of the Jacobian of the cost function with respect to the measurements. We will refer to this method as *Haralick's* method. In Censi (2007), this method was adapted to ICP which propagates the uncertainty from the measured sonar points to the scan matching solution. The author reported, using Monte Carlo simulations, similar results in corridors and circular scenarios and superior performance in square shaped environments. Hereafter, Haralick's method is adapted to our algorithm for which a closed form solution is proposed.

Let $\mathbf{a}_i = [a_{x_i}, a_{y_i}]^T \in S_{ref}$ be the corresponding point of $\mathbf{c}_i = [c_{x_i}, c_{y_i}]^T \in S_{new}$ and $\mathbf{q}_k = [x, y, \theta]^T$ the predicted displacement. Then, the robot displacement $\mathbf{q}_{min} = [x, y, \theta]^T$ can be estimated through the minimization of the error function $\mathbf{e}_i = \mathbf{a}_i - \mathbf{q}_k \oplus \mathbf{c}_i = \mathbf{a}_i - \mathbf{n}_i$ (as described in Algorithm 1):

$$\begin{aligned}\hat{\mathbf{q}}_{min} &= arg\ min_q \left\{ f\left(S_{ref}, S_{new}, \mathbf{q}_k\right)\right\} \\ &= arg\ min_q \left\{ \frac{1}{2}\sum_{i=1}^{n}\left(\hat{\mathbf{e}}_i^T \cdot \mathbf{P}_{e_i}^{-1} \cdot \hat{\mathbf{e}}_i\right)\right\} \end{aligned} \tag{14}$$

The method to propagate the uncertainties from the scan points to the scan displacement, independently from the minimization algorithm, only assumes that the cost function f has finite first and second partial derivatives with respect to sonar scan points $\mathbf{z} \equiv N\left(\hat{\mathbf{z}}, \mathbf{P}_\mathbf{z}\right)$ and to the scan displacement $\mathbf{q}_{min}$. If we take the partial derivatives of f with respect to $\mathbf{q}_{min}$, we can form the gradient g:

$$g\left(\mathbf{z}, \mathbf{q}_{min}\right) = \frac{\partial f\left(\mathbf{z}, \mathbf{q}_{min}\right)}{\partial \mathbf{q}_{min}} \tag{15}$$

where

$$\hat{\mathbf{z}} = [a_{x_1}, a_{y_1}, n_{x_1}, n_{y_1} \cdots a_{x_k}, a_{y_k}, n_{x_k}, n_{y_k}]^T \tag{16}$$

By taking the Taylor series expansion of g around $(\mathbf{z}, \mathbf{q})$ and taking into account that $\mathbf{q}_{min}$ is minimizing f and g, we can estimate the covariance $\mathbf{P}_\mathbf{q}$ of the $\hat{\mathbf{q}}_{min}$ as:

$$\mathbf{P}_{q_{min}} = \left(\frac{\partial g}{\partial \mathbf{q}_{min}}\right)^{-1} \cdot \frac{\partial g}{\partial \mathbf{z}} \cdot \mathbf{P}_\mathbf{z} \cdot \left(\frac{\partial g}{\partial \mathbf{z}}\right)^T \cdot \left(\frac{\partial g}{\partial \mathbf{q}_{min}}\right)^{-1} \tag{17}$$

where $\mathbf{P}_\mathbf{z}$ is a matrix consisting of the uncertainties of the scan points.

The formulation of the covariance of (14) in a closed form is not trivial since the construction of the necessary matrices depends on the cost function and the parameters. In the "Appendix", we present the closed-form expressions for calculating (17) in order to approximate the covariance of the scan matching estimation.

6 SLAM algorithm

The proposed pose-based SLAM algorithm uses an ASEKF for the scan poses estimation. In this implementation of the stochastic map (Smith et al. 1990), the estimate of the positions of the vehicle at the center of each full scan $\{\hat{\mathbf{x}}_1^B \ldots \hat{\mathbf{x}}_n^B\}$ at the time step (k) are stored in the state vector $\hat{\mathbf{x}}_k^B$, referenced to the base frame B:

$$\hat{\mathbf{x}}_k^B = \left[\left[\hat{\mathbf{x}}_{n_k}^B\right]^T \ \ldots \ \left[\hat{\mathbf{x}}_{i_k}^B\right]^T \ \ldots \ \left[\hat{\mathbf{x}}_{1_k}^B\right]^T\right]^T \tag{18}$$

and the covariance matrix for this state is defined as:

$$\mathbf{P}_k^B = E\left[(\mathbf{x}_k^B - \hat{\mathbf{x}}_k^B)(\mathbf{x}_k^B - \hat{\mathbf{x}}_k^B)^T\right] \tag{19}$$

For the reader's convenience, is reminded that a full scan is defined as the set of range measurements obtained after compounding all the robot poses with the 200 beams needed to obtain the full 360 deg sonar scan sector. As mentioned in Sect. 3, the output from the ScanGrabbing algorithm is a scan referenced at the center of that path. Each scan is considered rigid and is statistically independent as it has been build at a local frame.

6.1 Map initialization

All the elements of the state vector are represented in the map reference frame B. Although this reference frame can be defined arbitrarily, we have chosen to place its origin at the initial position of the vehicle at the beginning of the experiment and orient it to the North so compass measurements can be easily integrated.

The pose state $\mathbf{x}_i$ is represented as:

$$\mathbf{x}_i^B = [x \; y \; \psi]^T \tag{20}$$

where x, y and ψ are the position and orientation of the vehicle in the global frame B. The depth is not considered in this case as we build a planar map of the environment. The state and the map are initialized from the first available heading measurement.

6.2 Prediction

Let,

- $\mathbf{x}_{n-1_k}^B \equiv N(\hat{\mathbf{x}}_{n-1_k}^B, \; \mathbf{P}_k^B)$ be the last scan pose, and
- $\mathbf{q}_n^{B_n} \equiv N(\hat{\mathbf{q}}_n^{B_n}, \; \mathbf{P}_{q_n}^{B_n})$ be the robot displacement during the last scan, estimated through dead reckoning.

Then the prediction / state augmentation equation is given by:

$$\hat{\mathbf{x}}_{k+1}^{B^+} = \left[\left[\hat{\mathbf{x}}_{n-1_k}^B \odot \hat{\mathbf{q}}_{n_k}^{B_n}\right]^T \left[\hat{\mathbf{x}}_{n-1_k}^B\right]^T \cdots \left[\hat{\mathbf{x}}_{i_k}^B\right]^T \cdots \left[\hat{\mathbf{x}}_{1_k}^B\right]^T\right]^T \tag{21}$$

where, given that B and B_n frames are both North aligned, the operator $\odot$ is defined in the general case as:

$$\mathbf{x} \odot \mathbf{q} = \begin{bmatrix} a \\ b \\ c \end{bmatrix} \odot \begin{bmatrix} d \\ e \\ f \end{bmatrix} = \begin{bmatrix} a+d \\ b+e \\ f \end{bmatrix} \tag{22}$$

Being $\mathbf{A}_\odot$ and $\mathbf{B}_\odot$ the corresponding linear transformation matrices:

$$\mathbf{A}_\odot = \begin{bmatrix} \mathbf{I}_{2\times 2} & \mathbf{0}_{2\times 1} \\ \mathbf{0}_{1\times 2} & 0 \end{bmatrix}, \quad \mathbf{B}_\odot = \mathbf{I}_{3\times 3} \tag{23}$$

and being the predicted pose uncertainty $\mathbf{P}_{k+1}^{B^+}$ computed as:

$$\mathbf{P}_{k+1}^{B^+} = \mathbf{F}_k \mathbf{P}_k^B \mathbf{F}_k^T + \mathbf{G}_k \mathbf{P}_{q_n}^B \mathbf{G}_k^T \tag{24}$$

where,

$$\mathbf{F}_k = \begin{bmatrix} \mathbf{A}_\odot & \mathbf{0}_{3\times 3} & \cdots & \mathbf{0}_{3\times 3} \\ \mathbf{0}_{3\times 3} & \mathbf{I}_{3\times 3} & \cdots & \mathbf{0}_{3\times 3} \\ \vdots & \vdots & \cdots & \vdots \\ \mathbf{0}_{3\times 3} & \mathbf{0}_{3\times 3} & \cdots & \mathbf{I}_{3\times 3} \end{bmatrix}, \quad \mathbf{G}_k = \begin{bmatrix} \mathbf{B}_\odot \\ \mathbf{0}_{3\times 3} \\ \vdots \\ \mathbf{0}_{3\times 3} \end{bmatrix} \tag{25}$$

6.3 Scan matching measurement

In order to execute the modified pIC algorithm given two overlapping scans (S_i, S_n) with their related poses $(\mathbf{x}_i^B, \mathbf{x}_n^B)$, an initial guess of their relative displacement is necessary. This initial guess $[\hat{\mathbf{q}}_i^{I_i}, \mathbf{P}_{q_i}^{I_i}]$ can be easily extracted from the state vector using the tail-to-tail transformation (Smith et al. 1990):

$$\hat{\mathbf{q}}_i^{I_i} = \ominus \hat{\mathbf{x}}_i^B \oplus \hat{\mathbf{x}}_n^B \tag{26}$$

Since the tail-to-tail transformation is actually a non-linear function of the state vector $\mathbf{x}_k^B$, the uncertainty of the initial guess can be computed by means of the Jacobian of the non-linear function:

$$\mathbf{P}_{q_i}^{I_i} = \mathbf{H}_k \mathbf{P}_k^B \mathbf{H}_k^T \tag{27}$$

where

$$\mathbf{H}_k = \left.\frac{\partial \; \ominus \mathbf{x}_i^B \oplus \mathbf{x}_n^B}{\partial \; \mathbf{x}_k^B}\right|_{\hat{\mathbf{x}}_k^B} \tag{28}$$

Moreover, as shown in Smith et al. (1990), the Jacobian for the tail-to-tail transformation $\mathbf{x}_{a_c} = \ominus \mathbf{x}_{b_a} \oplus \mathbf{x}_{b_c}$, is:

$$\frac{\partial \; \ominus \mathbf{x}_{b_a} \oplus \mathbf{x}_{b_c}}{\partial \; (\mathbf{x}_{b_a} \mathbf{x}_{b_c})} = [\mathbf{J}_{1\oplus} \mathbf{J}_\ominus \;\; \mathbf{J}_{2\oplus}] \tag{29}$$

where $\mathbf{J}_{1\oplus}$, $\mathbf{J}_{2\oplus}$ and $\mathbf{J}_\ominus$ are the Jacobian matrices of the compounding and inverse transformations respectively.

As in our case $\mathbf{x}_{n_k}^B$ and $\mathbf{x}_{i_k}^B$ are components of the full state vector, the Jacobian of the measurement equation becomes:

$$\begin{aligned} \mathbf{H}_k &= \frac{\partial \; \ominus \mathbf{x}_{i_k}^B \oplus \mathbf{x}_{n_k}^B}{\partial \; \mathbf{x}_k} \\ &= \left[\mathbf{J}_{2\oplus_{3\times 3}} \;\; \mathbf{0}_{3\times 3(n-i-1)} \;\; \mathbf{J}_{1\oplus} \mathbf{J}_{\ominus_{3\times 3}} \;\; \mathbf{0}_{3\times 3(i-1)}\right] \end{aligned} \tag{30}$$

Once the initial displacement guess is available, the modified pIC algorithm can be used to produce an updated measurement of this displacement.

6.4 Loop closing candidates

Each new pose of a scan is compared against the previous scan poses that are in the nearby area (defined by a threshold) using scan matching. In order to avoid false positive registrations we define a percentage between the number of scan points that take part in the registration and the associated ones. Whenever enough points of the scans are overlapping the scan matching introduces a constraint between the poses updating the ASEKF. These constraints close the loops correcting the whole trajectory and bounding the drift.

Let,

- $\mathbf{x}_{n_k}^B$ be the last scan pose and S_{n_k} its corresponding scan,

- $Overlap_k = \left\{ S_{i_k} \;/\; \left\| \hat{\mathbf{x}}^B_{n_k} - \hat{\mathbf{x}}^B_{i_k} \right\| < threshold \right\}$ the set of overlapping scans and
- $\mathbf{O}_k = \left[S_{1_k},\ S_{2_k}\ \ldots\ S_{m_k} \right]$ the sequence of the overlapping scans belonging to the $Overlap_k$ set

Then $\forall\ [S_{i_k}, \mathbf{x}^B_i] \in \mathbf{O}_k$, perform a new scan matching between the scan poses $(\mathbf{x}^B_{n_k}, \mathbf{x}^B_{i_k})$ with the corresponding scans (S_{n_k}, S_{i_k}) obtaining $[\hat{\mathbf{q}}^{I_i}_i, \mathbf{P}^{I_i}_{q_i}]$ as the result of the scan matching. $\mathbf{P}^{I_i}_{q_i}$ is the corresponding uncertainty computed as described in Sect. 5. Finally the scan matching result is used to update the filter.

6.5 State update

When two overlapping scans (S_i, S_n) with the corresponding poses $(\mathbf{x}^B_i, \mathbf{x}^B_n)$ are registered, their relative displacement defines a constraint between both poses. This constraint can be expressed by means of the measurement equation, which in our case becomes:

$$\mathbf{z}_k = \ominus \mathbf{x}^B_{i_k} \oplus \mathbf{x}^B_{n_k} \tag{31}$$

where $\mathbf{x}^B_{i_k}$ is the scan pose which overlaps with the last scan pose $\mathbf{x}^B_{n_k}$. Now, an update of the stochastic map can be performed with the standard extended Kalman filter equations.

7 Experimental set-up and results

The validity of the scan matching SLAM technique described in the previous sections, has been tested with a dataset obtained by the *Ictineu* AUV in an abandoned marina.

7.1 Ictineu AUV

The Ictineu AUV has been designed and developed in the underwater robotics lab of the Universitat de Girona Spain. It was conceived around a typical open-frame design (see Fig. 6) as a research prototype for validating new technologies. It is a small (0.8 × 0.5 × 0.5 m), light (60 kg in air), and for very shallow water vehicle (depth rating 30 m). Although the hydrodynamics of open-frame vehicles is known to be less efficient than that of closed-hull type vehicles, they allow easy upgrades, sensors integration and maintenance. The vehicle is passively stable in roll and pitch due to the weight and volume distribution, and it can be controlled in surge, heave, and yaw with four thrusters (two for the surge and yaw, and two for the heave DOF). Two big cylindrical pressure vessels house the power and computer modules. The power module contains a pack of sealed lead acid batteries, which supply 24 Ah at 24 V and can provide the Ictineu AUV with more than 1 h of running time. The computer module has two PCs, one for control (PC104 AMD GEODE-300 MHz) and one for image and sonar processing (mini-ITX computer Via C3 1 GHz) connected through a 100 Mbps Ethernet switch. Table 1 reports the sensor suite of the vehicle as it was when collecting the dataset. The complete description of the Ictineu AUV at that time can be found in Ribas et al. (2007).

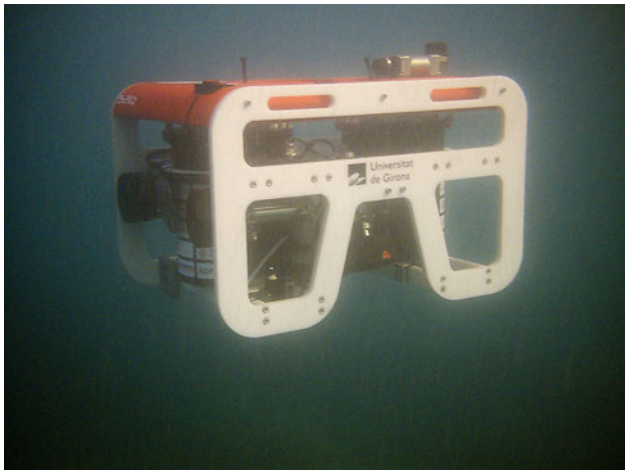

Fig. 6 The Ictineu AUV from University of Girona that was used for this work

Table 1 Summary of the Ictineu AUV sensor suite

Sensor	Model/specifications
Mechanical scanning imaging sonar	Tritech miniking
Max range:	100 m
Horizontal beamwidth:	3 deg
Vertical beamwidth:	40 deg
Scan rate (360-deg sector):	5–20 s
Frequency:	675 kHz
Doppler velocity log	Sontek Argonaut
Accuracy:	0.2 %
Frequency:	1.5 MHz
Max update rate:	10 Hz
Attitude and heading reference sensor	Xsens MTi
Static accuracy (roll/pitch):	<0.5 deg
Static accuracy (heading):	<1 deg
Max update rate:	256 Hz
Vision system	2 × B&W cameras
CCD size:	1/3 in.
Sensitivity:	0.01 lux
Color encoding system	PAL 576i
Orientation	Forward and down
Pressure sensor	Integrated to DVL
Range:	0–20 bar
Precision:	N.A.

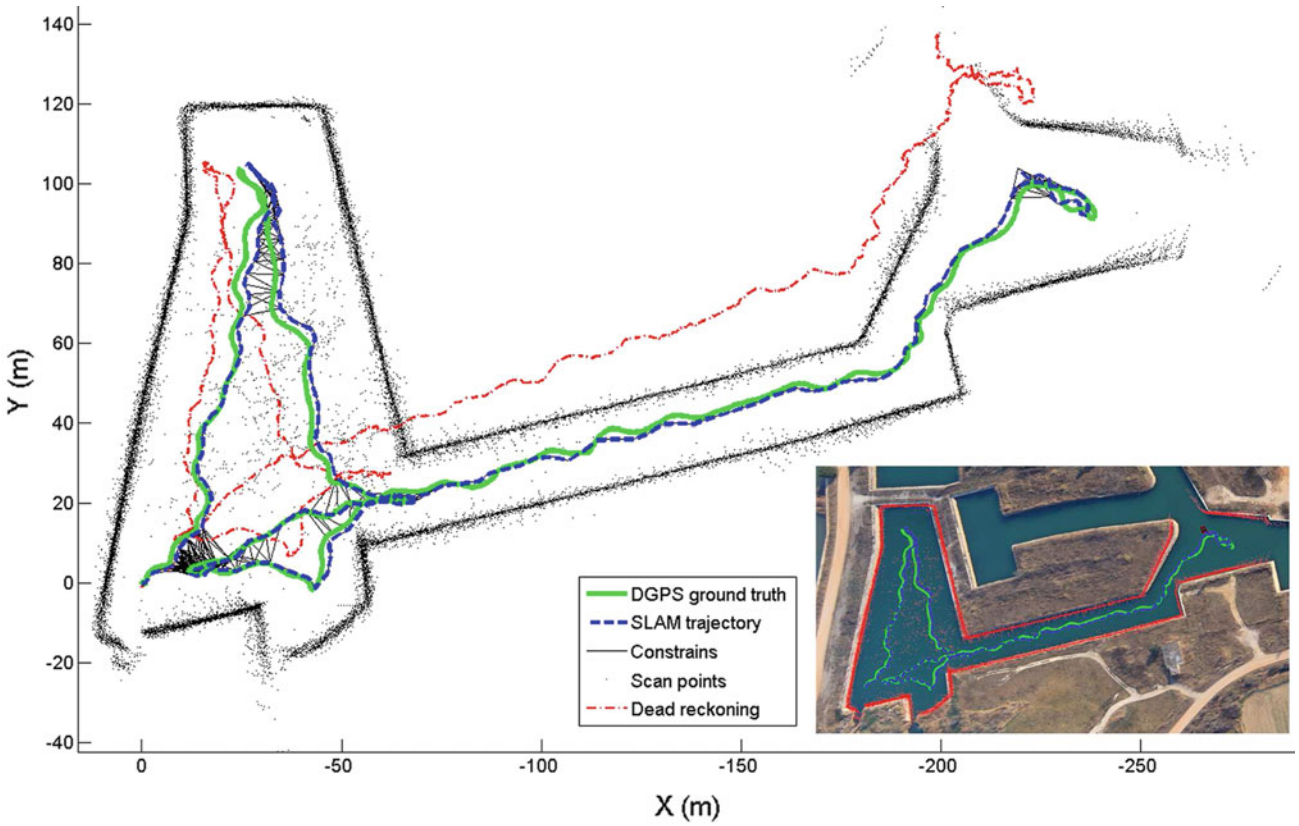

Fig. 7 SLAM Trajectory and map. In *red* (*dash-dot*) is the dead reckoning, in *green* (*solid*) *line* the DGPS trajectory used as a ground truth and in *blue* (*dash*) the trajectory estimated with the SLAM algorithm. In the *insert* is the trajectory and map projected on orthophoto image (Color figure online)

7.2 The marina dataset

The method described in this paper has been tested with a dataset obtained in an abandoned marina located at St. Pere Pescador, Costa Brava, Spain (Fig. 7, insert). This dataset is useful to test if an algorithm is capable to utilize the limited information provided by each scan in a large underwater environment and is available to the scientific community (Ribas et al. 2008). The dataset was obtained at a structured environment, however, our algorithm does not take into account any structural information or take advantage of existing features. In our current sensor configuration with an imaging sonar mechanically scanning the horizontal plane around the vehicle, the proposed method can be used wherever the surrounding vertical obstacles produce constant cross sections for the commanded operating depth.

The survey mission was carried out using the Ictineu AUV traveling along a 600 m path. The MSIS was configured to scan the whole 360 deg sector at a maximum range of 50 m, with a 0.1 m resolution and a 1.8 deg angular step. Dead reckoning can be computed using the velocity readings coming from the DVL and the heading data obtained from the AHRS sensor, both asynchronously. Standard deviation for the MSIS sensor was set at ± 0.1 m in range and ± 1.8 deg in angular measurements.

For evaluating the algorithm, a small buoy equipped with a DGPS sensor was attached on the top of the AUV, with a vertical separation of half meter. The AUV-buoy system was rigid and allowed the collection of ground truth data simultaneously with the acoustic data.

7.3 Results from the marina dataset

Figure 7 shows the trajectory and the map estimated with the proposed SLAM algorithm. In the insert, the results are projected on an orthophoto map of the real environment. As expected, the dead reckoning estimated trajectory suffers from a significant drift which is drastically limited by the SLAM algorithm. The inherent drift of the dead reckoning is significantly increased in our experiment by the combination of the low accuracy sensors that the vehicle were equipped (AHRS,DVL) and the strong presence of ferrous materials (cement walls) in the marina environment. These kind of perturbations and biases are very difficult to model in advance and are generally treated during post-processing. Nevertheless, our algorithm was able to correct the bias with-

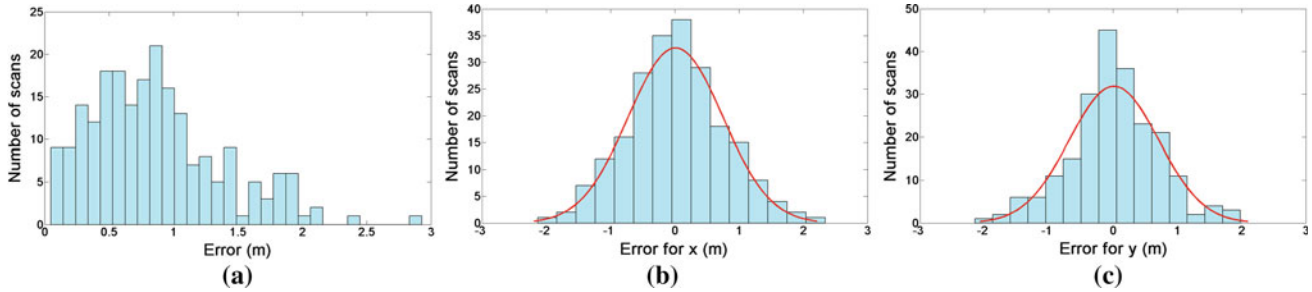

Fig. 8 Histograms of the error for all the scan displacements estimated through the SLAM and the corresponding displacement measured with the DGPS. **a** Absolute scan displacement error. **b** Error in X vectors. **c** Error in Y vectors. The *solid line* is the Gaussian fit to the histogram

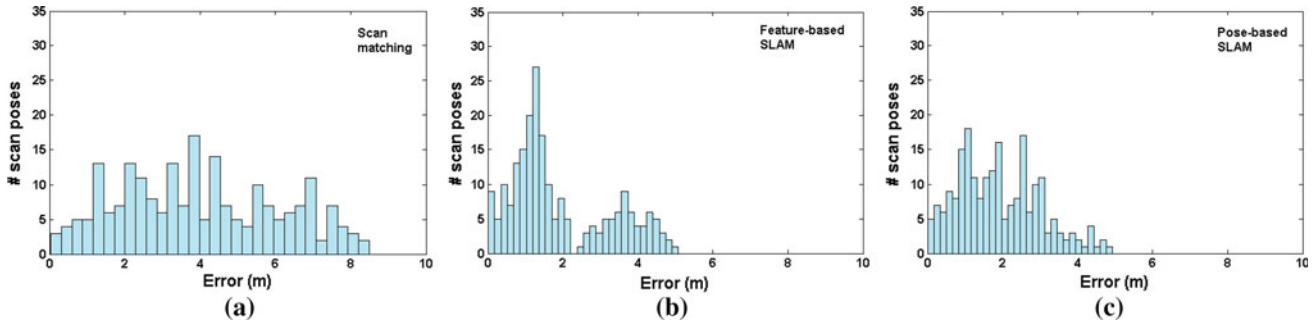

Fig. 9 Histograms of the absolute trajectory errors for: **a** pure scan matching, **b** feature-based SLAM and **c** pose-based SLAM

out any post-processing. The consistency of the algorithm can be appreciated also visually in the orthophoto map where the scan points and the trajectory are superimposed. The scan points fit the marina walls, except in those areas where the drift is higher (to the top right of the big tank, and at right at the end of the trajectory).

The whole dataset was acquired in 53 min with the vehicle traveling at 0.2 m/s average speed. The off-line execution of the proposed algorithm, implemented in MATLAB, takes around 14 min in a simple Pentium M @ 2.00 GHz laptop, which is 3.8 times shorter than the duration of the real experiment. It is reasonable to assume that an optimized implementation should be able to operate efficiently on-board the AUV.

The absolute scan displacement error for all scan poses can be seen in Fig. 8a. The absolute scan displacement error is computed as the difference between the displacement of a scan estimated through the SLAM algorithm and the corresponding displacement measured with the DGPS, assuming zero DGPS error. Figure 8b, c shows the histograms of the errors for the X and Y vectors and the solid line is the Gaussian fit to the histogram.

Figure 9 provides the absolute trajectory error between the results of dead reckoning, pure scan matching (Hernandez et al. 2009), feature-based SLAM (Ribas et al. 2008) and pose-based scan matching SLAM which is the current work. The absolute trajectory error is computed as the difference between the pose estimated through the SLAM algorithm and the corresponding pose measured estimated with the DGPS, assuming zero DGPS error. In Table 2 are summarized the mean, the standard deviation, the minimum and maximum of the absolute trajectory error for the methods we tested. As expected, both SLAM algorithms outperforms the pure scan matching implementation. The proposed pose-based scan matching SLAM has similar results with the feature-based SLAM. However, the main advantage of our algorithm lies to the fact that it does not rely on features or any structural information which has the potential to be applied in a natural environment.

Table 2 Error analysis between the current and previous algorithms by the authors

Method/error (m)	Mean	SD	Min.	Max.
Dead reckoning	17.46	11.47	0.09	45.42
Scan matching	3.99	2.11	0.03	8.49
Feature-based SLAM	1.91	1.32	0.01	5.08
Pose-based SLAM	1.90	1.09	0.01	4.93

We conclude the results with a note about the ground truth. The nominal accuracy of a DGPS is around 1 m and it degrades at an approximate rate of 0.22 m for each 100 km distance from the broadcast site (Monteiro et al. 2005). In this experiment, the vehicle was receiving differential corrections

from a nearby base station (< 40 km), therefor the theoretical DGPS drift is not more than 1.22 m. The execution of the algorithm has been visualized as shown in an animation (Online Resource 1).

8 Discussion and future work

The presented algorithm is composed of two main filters; one EKF at the local level of a scan estimating beam positions, and an ASEKF for estimating the position of the scans. In that sense, our algorithm is similar to the Hierarchical SLAM (Estrada et al. 2005) where the local submaps (scan in our case) are build to be independent, thus uncorrelated, and the higher level filter keeps the relative positions of the submaps without back-propagating corrections (updates) to them, as the submaps are relatively small. This same reasoning is applicable in our case, since the vehicle's motion during the building of a single scan is very small (a trajectory of 14 s with average speed of 0.2 m/s) and so any probable corrections from the higher level would have small effect to the scan precision. As the results show, our algorithm performs well with a slow moving vehicle, which is a reasonable assumption for an open-frame AUV. However, torpedo shaped AUVs are traveling with faster speeds and maybe face the situation where the dead reckoning estimation drifts significantly while a scan is formed. Future work will consider the performance of the algorithm for these situations.

Compared with our previous feature-based SLAM (Ribas et al. 2008), the proposed method has very similar results in the experimental dataset collected in an abandoned marina. However structured environments like an active marina will generally be populated with objects (boats, mooring lines) which are not easy to use as features because of their irregular shapes. Nonetheless, the algorithm described here does not take into account any structural information or extracting features. For this reason in a future work we will evaluate the algorithm in a more realistic or natural underwater environment.

9 Conclusions

In this paper we have developed a localization and mapping algorithm for an AUV, based on probabilistic scan matching of raw sonar scans within a pose-based SLAM framework. To deal with the motion-induced distortions affecting the generation of full sector scans, an EKF is used to estimate the robot motion during that scan. The filter uses a constant velocity model with acceleration noise for motion prediction. Velocities (DVL) and heading measurements (AHRS) arrive asynchronously and update the state. Through the compounding of the relative robot position within the scan with the range and bearing measurements of the beams gathered by the sonar, the sonar scan gets undistorted. Assuming Gaussian noise, the algorithm is able to estimate the uncertainty of the sonar measurements with respect to a frame located at the center of the scan.

For estimating the global trajectory of the vehicle, a second filter,an augmented state EKF, stores the pose of the vehicle where each full scan was completed. Each new full scan is cross registered with all the previous scans that are in a certain range, applying a modified pIC algorithm. This technique has a twofold effect: first, we get a better estimation of the vehicle's displacement that is used to update the ASEKF and at the same time, loop-closing events are updated. Furthermore, we present a closed form method for estimating the uncertainty of the scan matching result.

The proposed method has been tested with a real world dataset obtained in an abandoned marina during an engineering test mission. The results show the quality of our algorithm by comparing it to the ground truth from a GPS receiver and to other previously published algorithms.

Acknowledgments This research work was partially sponsored by the Spanish project DPI2011-27977-C03-02 (COMAROB) and two European Commission's Seventh Framework Program 2007-2013 Projects: ICT-248497 (TRIDENT) and Marie Curie PERG-GA-2010-276778 (Surf3DSLAM). The dataset was acquired with the help of the members (staff and students) of the Computer Vision and Robotics research group at the University of Girona.

Appendix

Index to electronic supplementary material

Online resource	Media type	Description
1	Video mpeg1	SLAM algorithm results in the marina dataset

Closed-form formulation of the scan matching uncertainty

A closed-form formula for propagating the uncertainty from matched image pairs to homography parameters describing the image motion for a 2D image mosaic optimization problem, is presented in Elibol (2011). The formula is based on the first order approximation for the bundle adjustment (BA) minimization algorithm. Hereafter, this method was adapted to the estimation of the covariance matrix of the scan matching displacement estimate.
Let,

– $\mathbf{z} \equiv N\left(\hat{\mathbf{z}}, \mathbf{P_z}\right)$, be the vector of the measured scan points assumed to be perturbed with a zero mean Gaussian ran-

dom noise. In our case, the scan matching does point-to-point association, therefore the measurements vector $\hat{\mathbf{z}}$ is a dimension of $4k \times 1$:

$$\hat{\mathbf{z}} = [\underbrace{a_{x_1}, a_{y_1}, n_{x_1}, n_{y_1}}_{\hat{\mathbf{z}}_1} \cdots \underbrace{a_{x_k}, a_{y_k}, n_{x_k}, n_{y_k}}_{\hat{\mathbf{z}}_k}]^T \tag{32}$$

and its covariance, given by $\mathbf{P_z}$, is a $(4k \times 4k)$ matrix consisted of the uncertainties of the scan points:

$$\mathbf{P_z} = \begin{bmatrix} \mathbf{P}_{a_1} & & \cdots & 0 \\ & \mathbf{P}_{n_1} & & \\ \vdots & & \ddots & \vdots \\ & & & \mathbf{P}_{a_k} \\ 0 & & \cdots & \mathbf{P}_{n_k} \end{bmatrix} \tag{33}$$

being block diagonal since the scan points are assumed to be uncorrelated. As a difference with laser scanners or multi-beam sonar profilers, using a rotating mono-beam sonar head, the scan points become correlated when represented in the scan I frame. Nevertheless, taking into account the short duration of the scan building process, the slow motion of the vehicle and without loss of generality, those correlations have been neglected in this work.

– $\mathbf{x}$ be the unknown parameters vector corresponding to the $\mathbf{q}_{min}$ estimated by the the pIC.

$$\mathbf{x} = [x, y, \psi]^T \tag{34}$$

– $f(\mathbf{z}, \mathbf{x})$ be an scalar, continuous, non-negative cost function of the overall square Mahalanobis distance of the matching error (from algorithm 1, line 13):

$$f(\mathbf{z}, \mathbf{x}) = \frac{1}{2} \sum_{i=1}^{k} \left(\mathbf{e}_i^T \cdot \mathbf{P}_{e_i}^{-1} \cdot \mathbf{e}_i \right) \tag{35}$$

Then, we can apply Haralick's method (Haralick 1998) in order to estimate the covariance $\mathbf{P_x}$ of the estimated $\hat{\mathbf{x}}$ which minimizes the above cost function (35):

$$\mathbf{P_x} = \left(\frac{\partial g}{\partial \mathbf{x}} \right)^{-1} \cdot \frac{\partial g}{\partial \mathbf{z}} \cdot \mathbf{P_z} \cdot \left(\frac{\partial g}{\partial \mathbf{z}} \right)^T \cdot \left(\frac{\partial g}{\partial \mathbf{x}} \right)^{-1} \tag{36}$$

where $g(\mathbf{z}, \mathbf{x}) = \left[\frac{\partial f(\mathbf{z}, \mathbf{x})}{\partial \mathbf{x}} \right]^T$. To do this, it is necessary to compute $g(\mathbf{z}, \mathbf{x})$, $\frac{\partial g(\mathbf{z}, \mathbf{x})}{\partial \mathbf{x}}$ and $\frac{\partial g(\mathbf{z}, \mathbf{x})}{\partial \mathbf{z}}$.

Let us begin rewriting the function (35) as:

$$f(\mathbf{z}, \mathbf{x}) = \frac{1}{2} \cdot \mathbf{R}^T \cdot \mathbf{W} \cdot \mathbf{R} \tag{37}$$

where $\mathbf{R}$ is the stacked vector of the measurement errors (of dimension $2k \times 1$):

$$\mathbf{R} = \left[\mathbf{e}_1^T \cdots \mathbf{e}_k^T \right]^T \tag{38}$$

and $\mathbf{W}$ is the inverted block diagonal matrix of the measurement errors covariances (of dimension $2k \times 2k$):

$$\mathbf{W} = blockdiag \left(\mathbf{P}_{e_1} \cdots \mathbf{P}_{e_k} \right)^{-1} \tag{39}$$

Because $\mathbf{W}$ is the inverse of a covariance matrix, it is positive definite and hence a Cholesky decomposition exists:

$$\mathbf{W} = \mathbf{L}^T \cdot \mathbf{L} \tag{40}$$

Now, for simplicity and without lost of generality, let us define:

$$\hat{\mathbf{R}} = \mathbf{L} \cdot \mathbf{R} \tag{41}$$

$\mathbf{W}$ is block diagonal because the scan points are assumed to be uncorrelated, so as is $\mathbf{L}$:

$$\mathbf{L} = blockdiag \left(\mathbf{L}_{e_1} \cdots \mathbf{L}_{e_k} \right) \tag{42}$$

Now, Eq. (37) can be rewritten as:

$$f(\mathbf{z}, \mathbf{x}) = \frac{1}{2} \cdot \hat{\mathbf{R}}^T \cdot \hat{\mathbf{R}} \tag{43}$$

and $g(\mathbf{z}, \mathbf{x})$ can be defined as the Jacobian of the cost function, being a (1×3) matrix;

$$g(\mathbf{z}, \mathbf{x}) = \frac{\partial f}{\partial x} = \hat{\mathbf{R}}^T \cdot \hat{\mathbf{J}}_x \tag{44}$$

where $\hat{\mathbf{J}}_x$ is the $(2k \times 3)$ Jacobian matrix of error vector $\hat{\mathbf{R}}$:

$$\hat{\mathbf{J}}_x = \frac{\partial \hat{\mathbf{R}}}{\partial \mathbf{x}} = \begin{bmatrix} \frac{\partial (\mathbf{L}_{e_1} \cdot \mathbf{e}_1)}{\partial x} & \frac{\partial (\mathbf{L}_{e_1} \cdot \mathbf{e}_1)}{\partial y} & \frac{\partial (\mathbf{L}_{e_1} \cdot \mathbf{e}_1)}{\partial \theta} \\ \vdots & \vdots & \vdots \\ \frac{\partial (\mathbf{L}_{e_k} \cdot \mathbf{e}_k)}{\partial x} & \frac{\partial (\mathbf{L}_{e_k} \cdot \mathbf{e}_k)}{\partial y} & \frac{\partial (\mathbf{L}_{e_k} \cdot \mathbf{e}_k)}{\partial \theta} \end{bmatrix} \tag{45}$$

The $\frac{\partial g(\mathbf{z}, \mathbf{x})}{\partial \mathbf{x}}$ is the (3×3) Hessian of $f(\mathbf{z}, \mathbf{x})$ and is calculated as follows:

$$\frac{\partial g}{\partial \mathbf{x}} = 2 \cdot \hat{\mathbf{J}}_{\mathbf{x}}^T \cdot \hat{\mathbf{J}}_{\mathbf{x}} + 2 \cdot \hat{\mathbf{R}}^T \frac{\partial \hat{\mathbf{J}}_{\mathbf{x}}}{\partial \mathbf{x}} \tag{46}$$

where $\frac{\partial \hat{\mathbf{J}}_{\mathbf{x}}}{\partial \mathbf{x}}$ is the $(6k \times 3)$ Hessian of $\hat{\mathbf{R}}$ which can be computed in the following way:

$$\frac{\partial \hat{\mathbf{J}}_{\mathbf{x}}}{\partial \mathbf{x}} = \frac{\partial}{\partial \mathbf{x}} \left(\frac{\partial \hat{\mathbf{R}}}{\partial \mathbf{x}} \right) = \sum_{i=1}^{3} \left(vec \left(\frac{\partial \hat{\mathbf{J}}_{\mathbf{x}}}{\partial x_i} \right) \right) \cdot \mathbf{r}_i^T \tag{47}$$

being $\mathbf{r}_i$ a (3×1) vector, with all zeros except its i^{th} row which is equal to 1. To compute the second part of (46), the (47) is multiplied by $\hat{\mathbf{R}}^T$ as follows:

$$\hat{\mathbf{R}}^T \frac{\partial \hat{\mathbf{J}}_{\mathbf{x}}}{\partial \mathbf{x}} = \left(\hat{\mathbf{R}}^T \otimes \mathbf{I}_3 \right) \cdot \frac{\partial \hat{\mathbf{J}}_{\mathbf{x}}}{\partial \mathbf{x}} \tag{48}$$

where $\otimes$ denotes Kronecker product of two matrices. Similarly, the $\frac{\partial g}{\partial \mathbf{z}}$ is a $3 \times 4k$ matrix, computed as:

$$\frac{\partial g}{\partial \mathbf{z}} = 2 \cdot \hat{\mathbf{J}}_{\mathbf{x}}^T \cdot \hat{\mathbf{J}}_{\mathbf{z}} + 2 \cdot \hat{\mathbf{R}}^T \frac{\partial \hat{\mathbf{J}}_{\mathbf{x}}}{\partial \mathbf{z}} \tag{49}$$

where $\hat{\mathbf{J}}_z$ is the Jacobian of the error vector $\hat{\mathbf{R}}$, being a $(2k \times 4k)$ matrix:

$$\hat{\mathbf{J}}_z = \frac{\partial \hat{\mathbf{R}}}{\partial \mathbf{z}} = \begin{bmatrix} \frac{\partial \hat{\mathbf{R}}_1}{\partial \mathbf{z}} & \cdots & 0 \\ \vdots & \ddots & \vdots \\ 0 & \cdots & \frac{\partial \hat{\mathbf{R}}_k}{\partial \mathbf{z}} \end{bmatrix} \tag{50}$$

where each $\frac{\partial \hat{\mathbf{R}}(i)}{\partial \mathbf{z}}$ is a (2×4) matrix, and $\frac{\partial \hat{\mathbf{J}}_{\mathbf{x}}}{\partial \mathbf{z}}$ is the following $(6k \times 4k)$ matrix:

$$\frac{\partial \hat{\mathbf{J}}_{\mathbf{x}}}{\partial \mathbf{z}} = \sum_{i=1}^{4k} \left(vec\left(\frac{\partial \hat{\mathbf{J}}_{\mathbf{x}}}{\partial \mathbf{z}_i} \right) \right) \cdot \mathbf{r}_i^T \tag{51}$$

being this time r_i a $(4k \times 1)$ vector of all zeros except its i_{th} row which is equal to 1. As previously, the second part of (49) is given by:

$$\hat{\mathbf{R}}^T \frac{\partial}{\partial \mathbf{z}} \left(\frac{\partial \hat{\mathbf{R}}}{\partial \mathbf{x}} \right) = \left(\hat{\mathbf{R}}^T \otimes \mathbf{I}_3 \right) \cdot \frac{\partial \hat{\mathbf{J}}_{\mathbf{x}}}{\partial \mathbf{z}} \tag{52}$$

References

Bailey, T., & Durrant-Whyte, H. F. (2006). Simultaneous localization and mapping (SLAM): Part II, state of the art. *IEEE Robotics and Automation Magazine*, *13*(3), 108–117.

Balsamo, A., Mana, G., & Pennecchi, F. (2006). The expression of uncertainty in non-linear parameter estimation. *Metrologia 43*(5):396–402. http://stacks.iop.org/0026-1394/43/i=5/a=009.

Barclay, L. (2003). *Propagation of radiowaves*. London: The Institution of Engineering and Technology.

Barkby, S., Williams, S., Pizarro, O., & Jakuba, M. (2009). An efficient approach to bathymetric SLAM. In *IEEE/RSJ international conference on intelligent robots and systems, IROS 2009* (pp. 219–224). doi:10.1109/IROS.2009.5354248.

Bar-Shalom, Y., & Fortmann, T. E. (1988). *Tracking and data association*. New York: Academic Press.

Bengtsson, O., & Baerveldt, A. J. (2003). Robot localization based on scan-matching—Estimating the covariance matrix for the IDC algorithm. *Robotics and Autonomous Systems, 44*(1), 29–40. doi:10.1016/S0921-8890(03)00008-3, best Papers of the Eurobot '01 Workshop.

Bülow, H., & Birk, A. (2011). Spectral registration of noisy sonar data for underwater 3d mapping. *Autonomous Robots*, *30*, 307–331. doi:10.1007/s10514-011-9221-8.

Bülow, H., Pfingsthorn, M., Birk, A. (2010). Using robust spectral registration for scan matching of sonar range data. In *7th symposium on intelligent autonomous vehicles (IAV)* IFAC.

Burguera, A., Oliver, G., & González, Y. (2010). Scan-based SLAM with trajectory correction in underwater environments. In *IEEE/RSJ international conference on intelligent robots and systems (IROS)* (pp. 2546–2551). doi:10.1109/IROS.2010.5649492.

Burguera, A., González, Y., & Oliver, G. (2008). A probabilistic framework for sonar scan matching localization. *Advanced Robotics*, *22*(11), 1223–1241.

Carpenter, R. N. (1998). Concurrent mapping and localization with FLS. In *Workshop on autonomous underwater vehicles*, Cambridge, MA, USA, pp. 133–148. doi:10.1109/AUV.1998.744449.

Castellani, U., Fusiello, A., Murino, V., Papaleo, L., Puppo, E., Repetto, S., & Pittore, M. (2004). *Efficient on-line mosaicing from 3D acoustical images*. OCEANS'04 MTTS/IEEE TECHNO-OCEAN'04 (Vol. 2, pp. 670–677).

Censi, A. (2007). An accurate closed-form estimate of ICP's covariance. In *Proceedings of the IEEE international conference on robotics and automation (ICRA)* (pp. 3167–3172). Rome, Italy. doi:10.1109/ROBOT.2007.363961, http://purl.org/censi/2006/icpcov.

Elibol, A. (2011). Efficient topology estimation for large scale optical mapping. Ph.D. thesis, University of Girona, Doctoral Programme in Technology.

Elibol, A., Gracias, N., & Garcia, R. (2010). Augmented state-extended Kalman filter combined framework for topology estimation in large-area underwater mapping. *Journal of Field Robotics*, *27*(5), 656–674. doi:10.1002/rob.20357.

Estrada, C., Neira, J., & Tardós, J. D. (2005). Hierarchical SLAM: Real-time accurate mapping of large environments. *IEEE Transactions on Robotics*, *21*, 588–596.

Eustice, R., Singh, H., Leonard, J., Walter, M., & Ballard, R. (2005). Visually navigating the RMS Titanic with SLAM information filters. In *Proceedings of robotics: Science and systems* (pp, 57–64). Cambridge, MA: MIT Press.

Fairfield, N., Kantor, G., & Wettergreen, D. (2007). Real-time SLAM with octree evidence grids for exploration in underwater tunnels. *Journal of Field Robotics*, *24*(1), 2.

Ferrer, J., Elibol, A., Delaunoy, O., Gracias, N., & Garcia, R. (2007). Large-area photo-mosaics using global alignment and navigation data. In *Proceedings of the Oceans MTS/IEEE*. Vancouber, Canada.

Foley, B., Sakellariou, D., Dellaporta, K., Bingham, B., Camilli, R., Eustice, R., et al. (2009). New methods for underwater archaeology: The 2005 Chios ancient shipwreck survey. *HESPERIA—Journal of the American Archaeological School at Athens*, *78*(2), 269–305. doi:10.2972/hesp.78.2.269.

Fossen, T. (1994). *Guidance and control of ocean vehicles*. New York: John Wiley and Sons Ltd.

Garcia, R., Cufi, X., Ridao, P., & Carreras, M. (2006). *Constructing photo-mosaics to assist UUV navigation and station-keeping*, AUTOMAR Thematic Network, Chap. Robotics and Automation in the Maritime Industries, pp. 195–234.

German, C., Connelly, D., Prien, R., Yoerger, D., Jakuba, M., Bradley, A., et al. (2004). *New techniques for hydrothermal exploration: In situ chemical sensors on AUVs—Preliminary results from the Lau Basin*. Trans Amer Geophys Union Fall Meet: EOS Supplement.

Haralick, R. (1998). Propagating covariance in computer vision. *Performance Characterization in Computer Vision*, *1*, 95–115.

Hernandez, E., Ridao, P., Ribas, D., & Batlle, J. (2009). MSISpIC: A probabilistic scan matching algorithm using a mechanical scanned imaging sonar. *Journal on Physical Agents (JoPhA)*, *3*(1), 3–12.

Hill, J., Driscoll, N., Weissel, J., Kastner, M., Singh, H., Cormier, M., et al. (2004). *A detailed near-bottom survey of large gas blowout structures along the US Atlantic shelf break using the autonomous underwater vehicle (AUV) SeaBED*. Trans Am Geophysical Union: EOS.

Johnson-Roberson, M., Pizarro, O., Williams, S., & Mahon, I. (2010). Generation and visualization of large-scale three-dimensional reconstructions from underwater robotic surveys. *Journal of Field Robotics*, *27*(1), 21–51.

Kinsey, J., Eustice, R., Whitcomb, L. (2006) .A survey of underwater vehicle navigation: Recent advances and new challenges. In *Proceedings of the 7th conference on maneuvering and control of marine craft (MCMC'2006)* IFAC, Lisbon.

Leonard, J. J., Carpenter, R. N., & Feder, H. J. S. (2001). Stochastic mapping using forward look sonar. *Robotica*, *19*(5), 467–480.
Leonard, J. J., & Feder, H. (2001). Decoupled stochastic mapping. *IEEE Journal of Oceanic Engineering*, *26*(4), 561–571.
Lu, F. (1995). *Shape registration using optimization for mobile robot navigation*. Ph.D. thesis, Department of C.S., University of Toronto.
Lu, Z., Hu, Z., & Uchimura, K. (2009). SLAM estimation in dynamic outdoor environments: A review. In M., Xie, Y., Xiong, C., Xiong, H., Liu, Z. Hu, (Eds.), *Intelligent robotics and applications, Lecture Notes in Computer Science* (Vol. 5928), Springer Berlin/Heidelberg, pp. 255–267.
Mahon, I., Pizarro, O., Johnson-Roberson, M., Friedman, A., Williams, S. B., & Henderson, J. C. (2011). Reconstructing Pavlopetri: Mapping the world's oldest submerged town using stereo-vision. In *IEEE International conference on robotics and automation, ICRA* (pp. 2315–2321).
Mahon, I., Williams, S., Pizarro, O., & Johnson-Roberson, M. (2008). Efficient view-based SLAM using visual loop closures. *IEEE Transactions on Robotics*, *24*(5), 1002–1014.
Mallios, A., Ridao, P., Ribas, D., Maurelli, F., & Petillot, Y., (2010). EKF-SLAM for AUV navigation under probabilistic sonar scan-matching. In *IEEE/RSJ International Conference on intelligent robots and systems (IROS), 2010* (pp. 4404–4411), doi:10.1109/IROS.2010.5649246.
Monteiro, L., Moore, T., & Hill, C. (2005). What is the accuracy of DGPS? *The Journal of Navigation*, *58*(02), 207–225.
Montesano, L., Minguez, J., & Montano, L. (2005). Probabilistic scan matching for motion estimation in unstructured environments. In *IEEE/RSJ international conference on intelligent robots and systems, (IROS 2005)* (pp. 3499–3504). doi:10.1109/IROS.2005.1545182.
Newman, P. M., Leonard, J. J., & Rikoski, R. J. (2003). Towards constant-time SLAM on an autonomous underwater vehicle using synthetic aperture sonar. In *Proceedings of the 11th international symposium on robotics research* Sienna, Italy.
Nieto, J., Bailey, T., & Nebot, E. (2007). Recursive scan-matching SLAM. *Robotics and Autonomous Systems*, *55*(1), 39–49. doi:10.1016/j.robot.2006.06.008.
Pfingsthorn, M., Birk, A., & Bulow, H. (2012). Uncertainty estimation for a 6-DoF spectral registration method as basis for sonar-based underwater 3D SLAM. In *IEEE international conference on robotics and automation (ICRA)* (pp. 3049–3054).
Pfister, S., Kriechbaum, K., Roumeliotis, S., & Burdick, J. (2002). Weighted range sensor matching algorithms for mobile robot displacement estimation. In *Proceedings of the IEEE international conference on robotics and automation, 2002. ICRA'02* (Vol. 2, pp. 1667–1674). doi:10.1109/ROBOT.2002.1014782.
Pizarro, O., Friedman, A., Johnson-Roberson, M., Williams, S., Mahon, I., Camilli, R., et al. (2010). High-resolution optical and acoustic 3D seafloor reconstructions from robot and diver-based surveys. In *XIX congress of the Carpathian–Balkan geological association, Carpathian–Balkan Geological Association* Abstracts volume (p. 314).
Reynolds, J., Highsmith, R., Konar, B., Wheat, C., & Doudna, D. (2001). Fisheries and fisheries habitat investigations using undersea technology. In *IEEE OCEANS-conference, 1998* (Vol. 2, pp. 812–820).
Ribas, D., Palomer, N., Ridao, P., Carreras, M., & Hernandez, E. (2007). Ictineu AUV wins the first SAUC-E competition. In: *IEEE international conference on robotics and automation* Roma, Italy.
Ribas, D., Ridao, P., Tardós, J., & Neira, J. (2008). Underwater SLAM in man made structured environments. *Journal of Field Robotics*, *25*(11–12), 898–921. doi:10.1002/rob.20249.
Roman, C., & Singh, H. (2005). Improved vehicle based multibeam bathymetry using sub-maps and SLAM. In *2005 IEEE/RSJ International Conference on intelligent robots and systems, 2005. (IROS 2005)* (pp. 3662–3669).
Singh, H., Armstrong, R., Gilbes, F., Eustice, R., Roman, C., Pizarro, O., et al. (2004). Imaging coral I: Imaging coral habitats with the SeaBED AUV. *Subsurface Sensing Technologies and Applications*, *5*(1), 25–42.
Singh, H., Roman, C., Pizarro, O., Eustice, R., & Can, A. (2007). Towards high-resolution imaging from underwater vehicles. *The International Journal of Robotics Research*, *26*(1), 55.
Smith, R., Self, M., & Cheeseman, P. (1990). *Estimating uncertain spatial relationships in robotics* (pp. 167–193). New York, NY, USA: Springer-Verlag New York, Inc.
Stutters, L., Liu, H., Tiltman, C., & Brown, D. (2008). Navigation Technologies for Autonomous Underwater Vehicles. *IEEE Transactions on Systems, Man, and Cybernetics, Part C: Applications and Reviews*, *38*(4), 581–589.
Tena, I., de Raucourt, S., Petillot, Y., & Lane, D. M. (2004). Concurrent mapping and localization using sidescan sonar. *IEEE Journal of Oceanic Engineering*, *29*(2), 442–456.
Walter, M., Hover, F., & Leonard, J. (2008). SLAM for ship hull inspection using exactly sparse extended information filters. In *IEEE international conference on robotics and automation, ICRA, 2008* (pp. 1463–1470).
White, C., Hiranandani, D., Olstad, C. S., Buhagiar, K., Gambin, T., & Clark, C. M. (2010). The malta cistern mapping project: Underwater robot mapping and localization within ancient tunnel systems. *Journal of Field Robotics*, *27*(4), 399–411. doi:10.1002/rob.20339.
Williams, S. B., Newman, P. M., Rosenblatt, J., Dissanayake, G., & Durrant-Whyte, H. (2001). Autonomous underwater navigation and control. *Robotica*, *19*(5), 481–496.

Angelos Mallios received the M.Sc. degree in industrial computing and automatic control from the University of Girona, Girona, Spain, in 2009, where he is currently working toward the Ph.D. degree in the Computer Vision and Robotics Group. From 1999 until 2007, he is with the Hellenic Centre for Marine Research (HCMR). He is also currently a member of the Research Center in Underwater Robotics (CIRS), University of Girona. His research interests include the simultaneous localization and mapping (SLAM) for AUVs, based on acoustic sensors and the technology advancements for underwater vehicles.

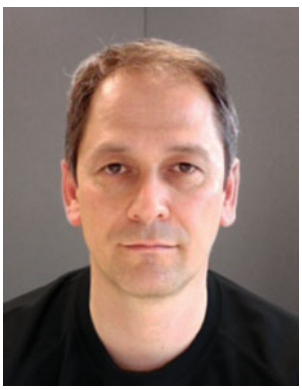

Pere Ridao received the Ms.C. degree in computer science from the Technical University of Catalonia, Barcelona, Spain, in 1993, and the Ph.D. degree in computer engineering from the University of Girona, Girona, Spain, in 2001. His research interests include underwater robotics in research topics such as intelligent control architectures, UUV modeling and identification, simulation, navigation, mission control, and real-time

systems. He is currently an Associate Professor in the Department of Computer Engineering, University of Girona, and the Head of the Research Center in Underwater Robotics (CIRS) at the same university. Dr. Ridao is also a member of the IFAC's Technical Committee on Marine Systems, a member of the Editorial Board of Springer's Intelligent Service Robotics journal, Secretary of the Spanish OES chapter, and also a board member of the Spanish RAS chapter.

David Ribas received the M.Sc. and Ph.D. degrees in industrial engineering from the University of Girona, Girona, Spain, in 2003 and 2008, respectively. In September 2003, he joined the Institute of Informatics and Applications, University of Girona, where he is currently a Researcher in the Department of Computer Engineering and a member of the Research Center in Underwater Robotics (CIRS). He is involved in national and European projects about underwater robotics and some technology transference projects about real-time and embedded systems. His research interests include the development of AUVs and more particularly the autonomous navigation problem using Simultaneous Localization and Mapping techniques.

Emili Hernández received his M.Sc. and Ph.D. degrees in computer engineering from the University of Girona, Spain. In 2005 he joined the Underwater Research Lab. of the Computer Vision and Robotics (VICOROB) Group of the University of Girona. He was a member of the Research Center in Underwater Robotics (CIRS) of Girona until March 2013. He is currently a postdoctoral research fellow in the Autonomous Systems Lab. at the CSIRO ICT-Centre, Australia. His research interests include path planning focused on autonomous underwater robots, sonar localization techniques and map building for online navigation purposes. He has been involved in several Local, National and European competitive research projects related with underwater robotics.